ISSN 1063-7842, Technical Physics, 2014, Vol. 59, No. 4, pp. 467–473. © Pleiades Publishing, Ltd., 2014.
Original Russian Text © A.E. Galashev, 2014, published in Zhurnal Tekhnicheskoi Fiziki, 2014, Vol. 84, No. 4, pp. 1–7.

THEORETICAL AND MATHEMATICAL PHYSICS

Computer Stability Test for Aluminum Films Heated on a Graphene Sheet

A. E. Galashev

Institute of Industrial Ecology, Ural Branch, Russian Academy of Sciences, ul. S. Kovalevskoi 20, Yekaterinburg, 620990 Russia
e-mail: galashev@ecko.uran.ru

Received May 14, 2013; in final form, September 12, 2013

Abstract—The behavior of single- and double-sided monatomic aluminum films on graphene heated from 300 to 3300 K is studied by the molecular dynamics method. Atoms of single-sided coating are preserved on graphene up to 3300 K, while atoms of double-sided coating leave graphene even at 1800 K; upon a further increase in temperature, this leads to an increase in the horizontal and vertical components of the self-diffusion coefficient. The stresses produced by vertical forces are found to be most significant in metallic films; these stresses almost disappear when temperature reaches 2300 K. The stresses in graphene, the highest of which are concentrated in the zone of formation of the metal film, substantially decrease upon heating.

DOI: 10.1134/S1063784214040112

INTRODUCTION

Aluminum films are widely used as protective coatings for components of various devices owing to their high chemical stability [1]. The mechanical strength of thin films is often much lower as compared to that of the corresponding bulk material. Such films can be reinforced significantly by using graphene, which is a monolayer material with unique strength properties. Graphene also has an extremely high melting point (~4900 K) [2], which raises the hope that aluminographene coatings can be used at still higher temperatures than purely aluminum coatings with a melting point of 933 K. The high electron mobility and ultrahigh thermal conductivity of graphene was demonstrated experimentally in [3] and [4, 5], respectively. To improve the thermal properties of aluminum coatings, ultrathin AlN films were used [6]. However, these films exhibited chemical instability to the formation of aluminum hydroxide in water at 373 K and to the formation of Al_2O_3 at 1273 K in air. In addition, the roughness of AlN film coatings was four times higher than that of an Al_2O_3 coating.

Interest in experimental investigations of ultrathin aluminum films on graphene has considerably increased in recent years [7–9]. At the same time, these objects have not been comprehensively investigated theoretically. Coating of graphene oxide with a thin aluminum film makes it possible to generate a high acousto-optical pressure due to optimization of thermal elasticity produced by the metal film as well as thermal conductivity exhibited by graphene oxide [7]. Ultrathin films obtained by deposition of aluminum oxide on graphene are characterized by a very high strength [8]. Such films can be used as thin-film coatings, membranes, and in flexible electronics. The dielectric properties of a naturally oxidized aluminum film on graphene make it possible to use it for preparing electric shutters [9].

In actual experiments, it is difficult to control nanoscratches and nanodents. Such difficulties can easily be eliminated using molecular-dynamic (MD) simulation. This method is widely used for studying friction and cracks in thin films [10, 11]. On the basis of MD simulation, the elastoplastic deformation on the surface of a nickel single crystal was considered as nucleation of dislocations [12].

This study aims at investigation of the effect of high temperatures on the structure and kinetic and mechanical properties of monolayer aluminum films deposited on a graphene sheets by the molecular dynamics method.

1. COMPUTER MODEL

The potential model of graphene used here was developed on the basis of the Morse [13], Abel [14], and Tersoff potentials [15–17] and also modifications proposed in [18]. Potential function U was defined as

$$U = \sum_{i,j>1}[V_{ij}^R(r_{ij}) - b_{ij}(\{\mathbf{r}\}, \{\theta^B\}, \{\theta^{DH}\})V_{ij}^A(r_{ij})], \quad (1)$$

where r_{ij} are the distances between the ith and jth atoms and function b_{ij} represents multiparticle connection between the i–j coupling and the local surrounding of the ith atom. Coupling angle θ_{ijk}^B is defined as the angle between vectors $\mathbf{r}_{ji}$ and $\mathbf{r}_{ik}$:

$$\cos\theta_{jik}^B = \frac{\mathbf{x}_{ji}\mathbf{x}_{ki}}{r_{ji}r_{ki}}, \quad (2)$$

where $\mathbf{x}_{ji}$ is the coordinate vector directed from the jth to the ith atom.

Dihedral angle θ^{DH}_{kijl} is defined as the angle between the plane passing though the jth, ith, and kth atoms and the plane passing though the ith, jth, and lth atoms. The cosine of angle θ^{DH}_{kijl} is defined as

$$\cos\theta^{DH}_{kijl} = \frac{\mathbf{x}_{ik}\times\mathbf{x}_{ji}}{r_{ik}r_{ji}}\frac{\mathbf{x}_{ji}\times\mathbf{x}_{lj}}{r_{ji}r_{lj}}. \qquad (3)$$

The potential components V^R_{ij} and V^A_{ij} describing repulsion and attraction, respectively, were determined using the Morse potential [15–17]. As compared to [15–17], we have increased the coupling distance from 0.21 to 0.23 nm, having preserved the remaining parameters of the potential describing the C–C interactions. We also used the weak Lennard–Jones attraction with the parameters from [18] to take into account the C–C interaction at distances $r_{ij} >$ 0.23 nm.

The Al–Al interaction was represented by the Sutton–Chen potential [19]

$$U^{SC} = \varepsilon\left[\frac{1}{2}\sum_i\sum_{j\neq i}V(r_{ij}) - c\sum_i\sqrt{\rho_i}\right], \qquad (4)$$

where

$$V(r_{ij}) = (a/r_{ij})^n, \qquad (5)$$

$$\rho_i = \sum_{j\neq i}(a/r_{ij})^m. \qquad (6)$$

Parameters ε, a, c, m, and n of potential U^{SC} are given in [19]. The Al–C interactions were described by the Morse potential with the parameters established in [20].

The stress at the site of an atom in a metal film is defined as [19]

$$\sigma_{\alpha\beta}(i) = \frac{\varepsilon}{2a^2\Omega_i}\sum_{i\neq j}^{k}[-n(a/r_{ij})^{n+2} + mc(1/\sqrt{\rho_i} + 1/\sqrt{\rho_j})(a/r_{ij})^{m+2}]r^{\alpha}_{ij}r^{\beta}_{ij}, \qquad (7)$$

where Ω_i is the volume corresponding to an individual atom, which can be associated with the volume of the Voronoy polyhedron connected with the ith atom.

To calculate the stresses emerging in graphene, the graphene sheet was divided into elementary area elements. Atomic stresses $\sigma^i_J(n)$ on the nth area element for each of directions x, y, and z with running index J were determined by calculating the kinetic energies of atoms on this area element and projections f^i_J of the forces exerted on the nth area element by all other atoms,

$$\sigma^i_J(n) = \frac{1}{k}\left\langle\sum_i^k\frac{1}{\Omega}(m v^i_J v^i_J)\right\rangle + \frac{1}{S_n}\left\langle\sum_i^k f^i_J\right\rangle, \qquad (8)$$

where k is the number of atoms on the nth area element, Ω is the volume per atom, m is the mass of the atom, v^i_J is the J projection of the velocity of the ith atom, and S_n is the area of the nth element. Angle brackets $\langle\ldots\rangle$ denote averaging over time. Compressive stresses with such a definition may have the $\langle+\rangle$ or $\langle-\rangle$ sign depending on the direction of forces f^i_J. This forms the difference between microscopic stress $\sigma^i_J(n)$ and macroscopic stress $\bar{\sigma}_J < 0$.

Initially, Al atoms were on the graphene sheet in the form of a loose (111) plane in the fcc lattice (parallel to the graphene plane) with distance $r_{\text{Al–Al}} = 0.6336$ nm between the nearest atoms. In this case, Al atoms were strictly opposite to the centers of hexagonal cells formed by carbon atoms, and the shortest spacing $r_{\text{C–Al}} = 0.248$ nm between the C and Al atoms corresponded to the value of $r_{\text{C–Al}}$ calculated using the density functional theory [21]. In the bulk aluminum crystal, we have $r_{\text{Al–Al}} = 0.2857$ nm. Consequently, the Al films were initially in the stretched state resulting from the incompatibility of the lattice periods of graphene and aluminum. The shortest distance between C atoms in graphene is $r_{\text{C–C}} = 0.142$ nm. We analyze here two systems; system I is the aluminum film on monolayer graphene, while system II corresponds to a graphene monolayer coated on both sides with identical Al films. Integration of the equation of motion was performed using the fourth-order Runge–Kutta method with time step $\Delta t = 0.2$ fs. The computer time for each value of temperature was $10^6\,\Delta t$ or 200 ps. The computations were started at a temperature of 300 K. After each million of time steps, the temperature of the system was elevated by 500 K, and the next computation of the same duration was carried out. The last computation corresponded to 3300 K. The temperature in the model was maintained with the help of the Berendsen thermostat [22].

The spectrum of individual oscillations of atoms is defined as the Fourier transform of the average autocorrelation function of velocities,

$$f(\omega) = \frac{2M}{3\pi kT}\int_0^{\infty}\langle\mathbf{v}(0)\mathbf{v}(t)\rangle\cos(\omega t)dt, \qquad (9)$$

where M is the mass of an atom and k is the Boltzmann constant.

The self-diffusion coefficient was defined in terms of the mean square of atomic displacements $\langle|\Delta\mathbf{r}(t)|^2\rangle$ as

$$D = \lim_{t\to\infty}\frac{1}{2\Gamma}\langle[\Delta\mathbf{r}(t)]^2\rangle, \qquad (10)$$

where Γ is the dimensionality of the space.

2. TESTING OF THE METHOD AND MODEL

It was shown in a separate computation that the application of the fourth-order Runge–Kutta method ensures higher accuracy in determining atomic trajectories as compared to the result obtained using the same method of the second order. In addition, the second-order algorithm is less stable and necessitates a reduction of the time step. The application of the fourth-order algorithm ensures the optimal balance between the time step and the accuracy of computations. The computational error in the MD method is mainly determined by the systematic error depending on the integration procedure used [23, 24]. Total computation time $t_0 = 200$ ps exceeded characteristic correlation time t_m for coupling functions in graphene and in the metal. Time t_m is on the order of the ratio of the film layer thickness to the speed of sound and is characterized as the stabilization time of incomplete equilibrium for the quantity in question. Assuming that the speed of sound is 5 km/s in aluminum and $u_\perp = 15$ km/s, $u_\Updownarrow = 21$ km/s in graphene [25] and estimating the sizes of atoms from the geometrical Lennard–Jones parameter, we find that $t_m < 0.2$ ps even for duplitized aluminum film on graphene. It can be expected that the computational error for the coordinates, velocities, and autocorrelation functions [23, 24] and the Fourier transform of the spectra obtained in terms of these quantities does not exceed $(t_m/t_0)^{3/2} \approx 5 \times 10^{-5}$. The error in the computation of the total energy in terms of its fluctuations can be estimated as $\sqrt{\langle \Delta E^2 \rangle / E} \approx 0.1$.

The resistivity of the pure metal in the simplified approximation can be defined as [26]

$$\rho(T) = \left(\frac{m}{2}\right)^{1/2} \frac{9\pi h^2 C^2}{8n\Omega e^2 Mk\Theta\zeta^{3/2}} \left(\frac{T}{\Theta}\right)^5 \times \int_0^{\Theta/T} \frac{z^5 dz}{(\exp(z)-1)(1-\exp(-z))}. \tag{11}$$

Here, ζ is the Fermi energy level $\left(z = \frac{1}{2} m\bar{v}^2\right)$, Θ is the Debye temperature, Ω is the unit cell volume, C is the constant determining the interaction between electrons and the lattice, h is the Planck constant, and $z = \hbar\omega/kT$.

When the electrical conductivity (or another transport parameter) is calculated, constant C can be determined from the relation [27]

$$\lambda_{\text{tr}} = 2 \int_0^{\omega_{\max}} C^2 \frac{F(\omega)}{\omega} d\omega, \tag{12}$$

where $F(\omega)$ is the phonon spectrum, $\omega_{\max}$ is the maximal frequency in the phonon spectrum under investigation, and $\lambda_{\text{tr}} = 0.39$ is the transport constant of the electron–phonon coupling in aluminum [27]. In the Debye model, the phonon density of states is defined as

$$F(\omega) = 9\omega^2/\omega_{\text{D}}^3, \tag{13}$$

where $\omega_{\text{D}} = \Theta k/\hbar$ is the cutoff frequency of the Debye spectrum.

The resistivity of a single-layer aluminum film at 300 K, calculated by formula (11), is $\rho = 0.185 \times 10^{-4}\ \Omega$ m, and electrical conductivity is $\sigma = 5.4 \times 10^4\ \Omega^{-1}$ m^{-1}. The electrical conductivity of a thin metal film can be written in the form [28]

$$\sigma = \sigma_0 \exp(-E_{\text{ac}}/kT), \tag{14}$$

where σ_0 is the conductivity of the bulk material and E_{ac} is the activation energy for conduction electrons. Assuming that the conductivity of bulk aluminum is $\sigma_0 = 0.37 \times 10^8\ \Omega^{-1}$ m^{-1}, we obtain from expression (14) $E_{\text{ac}} = 0.098$ eV. The temperature coefficient $\beta = \frac{1}{\rho}\frac{d\rho}{dT}$ of the resistance of a monolayer Al film determined from the calculation of ρ at temperatures of 300 and 800 K is found to be 4×10^4 K^{-1}. The electric properties of thin aluminum films with a thickness from 40 to 200 nm deposited on a glass substrate at 573 K in high vacuum were studied experimentally in [28]. The surfaces of the layers deposited one by one were subjected to the action of oxygen. Extrapolation of functions $\rho(d)$ and $\beta(d)$, where d is the film thickness, to a thickness of an atomic monolayer leads to values of $2.5 \times 10^{-4}\ \Omega$ m and 3×10^3 K^{-1}, respectively. Therefore, the values of the conductivity and activation energy of conduction electrons extrapolated from experiments are $\sigma = 0.4 \times 10^4\ \Omega^{-1}$ m^{-1} and $E_{\text{ac}} = 0.168$ eV. The experimentally obtained lower conductivity and higher activation energy can be explained by oxidation and a higher temperature of the experimental sample, the extrapolation error, the roughness of calculation of ρ by formula (11), and the large temperature step in the computation of β.

The total energy of free one-sheet graphene obtained in our MD experiment at $T = 300$ K was -7.02 eV, which is in conformity with the result of quantum-mechanical calculation (-6.98 eV) [29]. The aluminum–graphene interaction energy $E_{\text{Al–C(graphene)}}$ in the MD model at this temperature is -0.225 eV. The density functional theory for the interaction between the Al (111) plane and graphene gives $E_{\text{Al–C(graphene)}} = -0.185$ eV [21]. Heat capacity c_V of the single-sheet graphene calculated in terms of kinetic energy fluctuations increases in the temperature interval 300 K $\le T \le$ 1300 K from 19 to 28 J/mol K, which corresponds to experimental values of this quantity (23.74–26.80 J/mol K) [30].

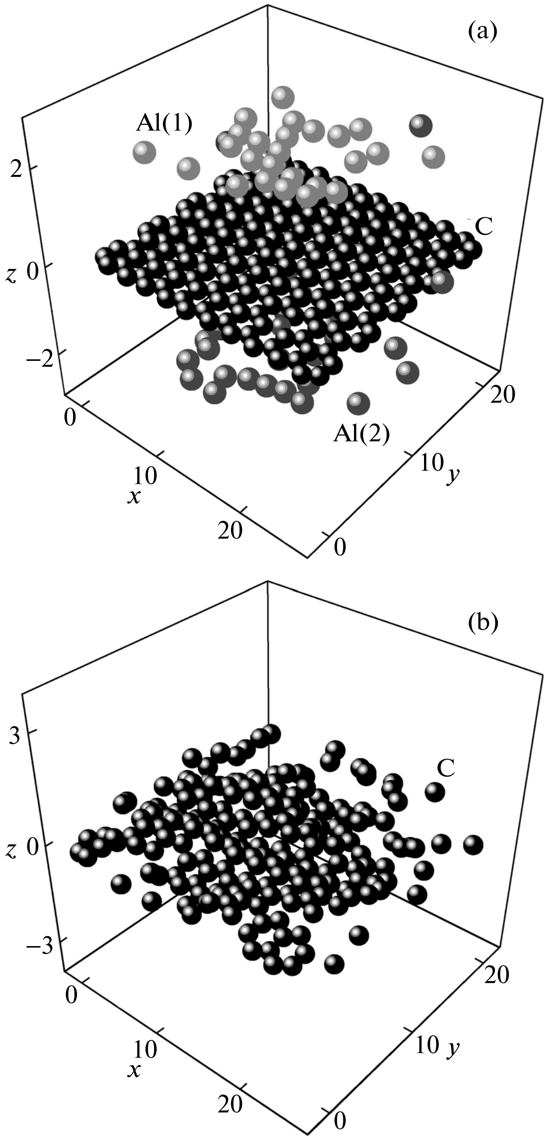

Fig. 1. Configurations of the system formed by two aluminum films on the graphene sheet, corresponding to different temperatures: (a) 300 K; (b) 3300 K at an instant of 200 ps; the coordinates are measured in angstroms.

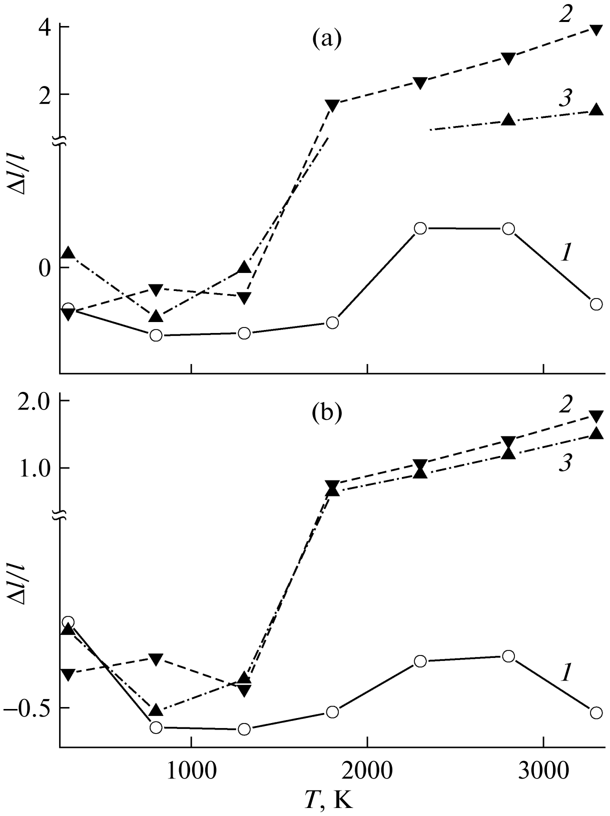

Fig. 2. Relative elongation of Al films in (a) longitudinal (*x*) and (b) transverse (*y*) directions for systems consisting of a single Al film on a graphene sheet (*1*), top (*2*) and bottom (*3*) Al films on the graphene sheet with double-sided coating.

3. RESULTS OF COMPUTATION

The atomic configurations of system II at the initial (300 K) and final (3300 K) temperatures are shown in Fig. 1. Even at 300 K, Al atoms on the top side of the graphene sheet form a planar loose droplet without moving over appreciable distances from the sheet surface. At the same time, Al atoms located at the bottom part of the sheet are also grouped; however, some of these atoms can move over considerable distances both in the vertical and in horizontal directions. The convergence of Al atoms on both sides of the graphene sheet appears as natural because their initially loose packing did not correspond to the condensed state in which the system should be under such conditions. A small part of the lower Al atoms can move round the graphene sheet and come up. One such atom joined the upper group of Al atoms. Figure 1b shows the same volume of space as in Fig. 1a at 3300 K. It can be seen that not a single atom of the metal remained in the immediate vicinity of the graphene sheet. At this temperature, considerable changes in the structure of the graphene sheet are observed. First of all, the sheet edges are damaged. The central part of the sheet is still dense, but the hexagonal cellular structure in this part is manifested less clearly.

The Al atoms of system II leave the graphene sheet at a temperature of 1800 K, while all atoms of system I remain in the vicinity of the graphene sheet even at 3300 K. The relative elongation of the Al films in the longitudinal (*x*) and transverse (*y*) directions is shown in Fig. 2. The direction of the *x* axis corresponds to the "zigzag" direction of the graphene sheet, while the direction of the *y* axis coincides with the "chair" direction. The longitudinal and transverse sizes of the films were determined by averaging the atomic positions of the corresponding opposite edges of the films. In both systems, Al films exhibited contractions in the longitudinal and transverse directions up to 1300 K

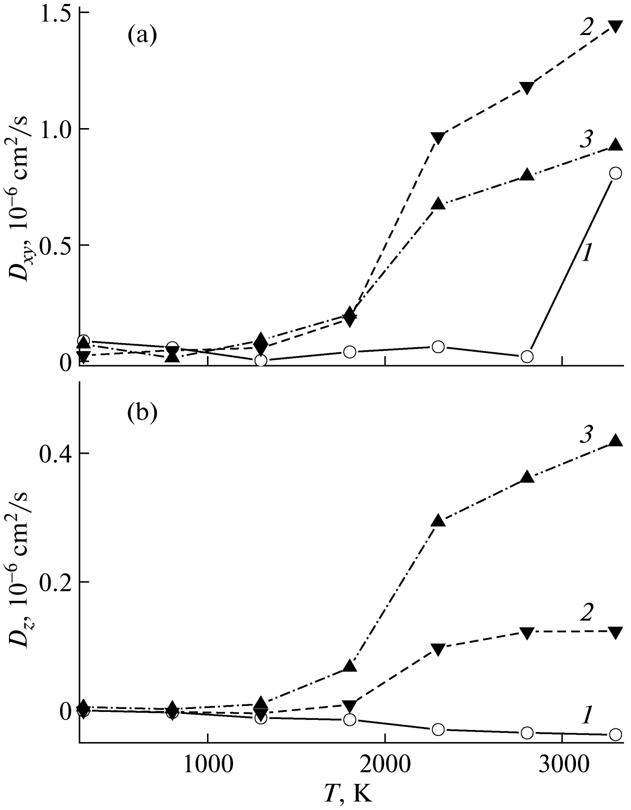

Fig. 3. (a) Horizontal D_{xy} and (b) vertical D_z components of the self-diffusion coefficient of Al films: single Al film on the graphene sheet (*1*), top (*2*) and bottom (*3*) Al films on the graphene sheet with double-sided coating.

(the values of $\Delta l/l$ were negative). The only exception was the longitudinal size of the lower film in system II at $T = 300$ K, where $\Delta l/l > 0$. The positive values of $\Delta l/l$ for the Al film in system I were observed only at 2300 and 2800 K exclusively in the longitudinal direction. Thus, double-sided coating of the graphene sheet by stretched monolayer Al films considerably reduces thermal stability of these films relative to the corresponding single-sided coating. This is due to the strong repulsive interaction between Al atoms in the vicinity of $T = 1800$ K in the case of insufficiently strong binding of aluminum with graphene.

Figure 3 shows the temperature dependences of horizontal (D_{xy}) and vertical (D_z) components of the self-diffusion coefficient of the metal films under investigation. For the Al film coating one side of the graphene sheet, the value of D_{xy} first decreases up to $T = 1300$ K, and then the $D_{xy}(T)$ dependence passes through a small peak (at $T = 2300$ K). Finally, the values of D_{xy} sharply increase when a temperature of 3300 K is approached. The decrease in D_{xy} is associated with the compaction of Al atoms on the substrate. The melting point of bulk aluminum obtained in actual experiments is 933 K, and its experimental boiling point corresponds to 2773 K. The Al film passes to the liquid state at $T = 1300$ K. The large variety of structures in the liquid state leads to the emergence of the peak on the $D_{xy}(T)$ curve. At a temperature of 2800 K, the Al film passes to the state in which metal atoms begin to evaporate. As a result, the D_{xy} component of this film increases significantly. The behavior of quantity D_{xy} for Al films coating both sides of the graphene sheet is different. Such films exhibit an insignificant increase in the D_{xy} component upon heating from 800 to 1800 K. A sharp increase in D_{xy} is observed near 2300 K, which is followed by a significant increase in the horizontal mobility at higher temperatures. The D_z component for system I decreases upon heating. This is due to the formation of a dense flat Al droplet on the surface of the graphene sheet. Collective adhesion of Al atoms with the sheet surface reduces the vertical component of the self-diffusion coefficient. Analogous adhesion is also observed for Al films in system II, but only up to a temperature of 1300 K. The attraction of Al atoms belonging to different films at high temperatures leads to strong collisions of metal atoms with the substrate; as a result, Al atoms acquire large vertical velocity components, and the D_z component increases rapidly.

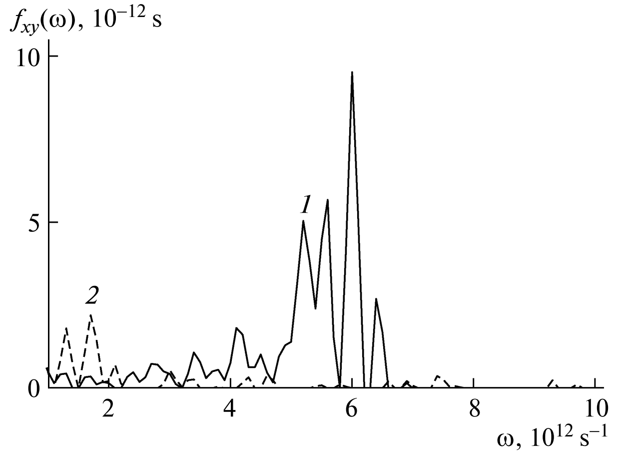

Fig. 4. Frequency spectra of individual vibrations of Al atoms in the *xy* plane: top (*1*) and bottom (*2*) films at 1300 K.

Let us now consider the change in the vibrational motion of Al atoms after the addition of the second (bottom) metal film to the graphene sheet. The frequency spectra of vibrations of Al atoms in the *xy* plane for the film in system II at 1300 K are shown in Fig. 4. At this temperature, most Al atoms in system II are still in the vicinity of the graphene sheet. The frequency spectrum for Al atoms of the top film has four intense peaks in the frequency interval $(5.0 \leq \omega \leq 6.5) \times 10^{12}$ s^{-1}. At lower frequencies, the intensity of the peaks decreases. Conversely, the intensity of the peaks for the bottom film in this frequency interval is minimal, while the peaks localized at the lowest frequencies (1.3×10^{12} and 1.7×10^{12} s^{-1}) have the maximal intensity. Thus, as a result of the separation of a small

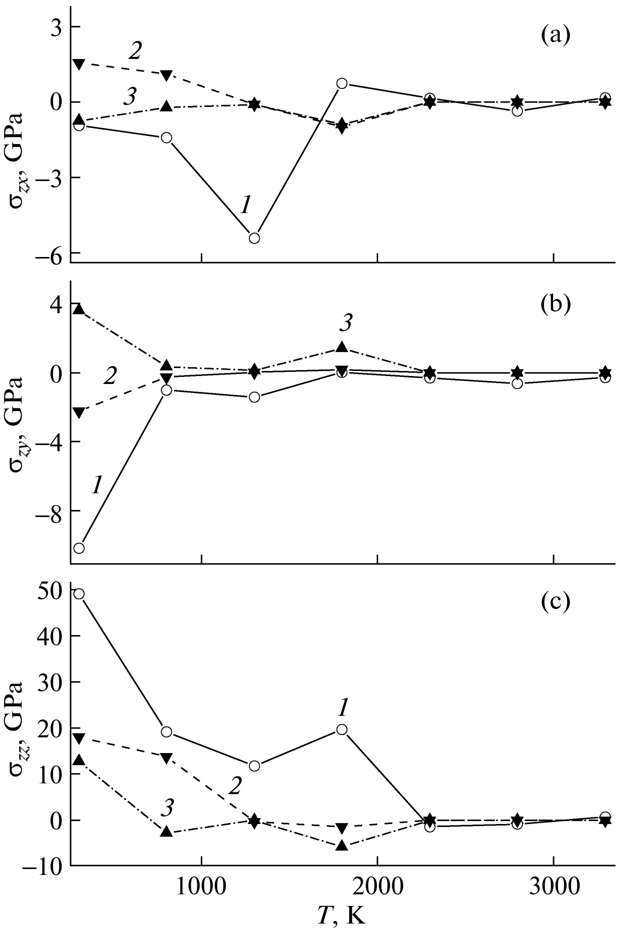

Fig. 5. Stresses (a) σ_{zx}, (b) σ_{zy}, and (c) σ_{zz} in the *xy* plane of the metal film for systems with a single Al film on the graphene sheet (*1*), top (*2*) and bottom (*3*) Al films on the graphene sheet with double-sided coating.

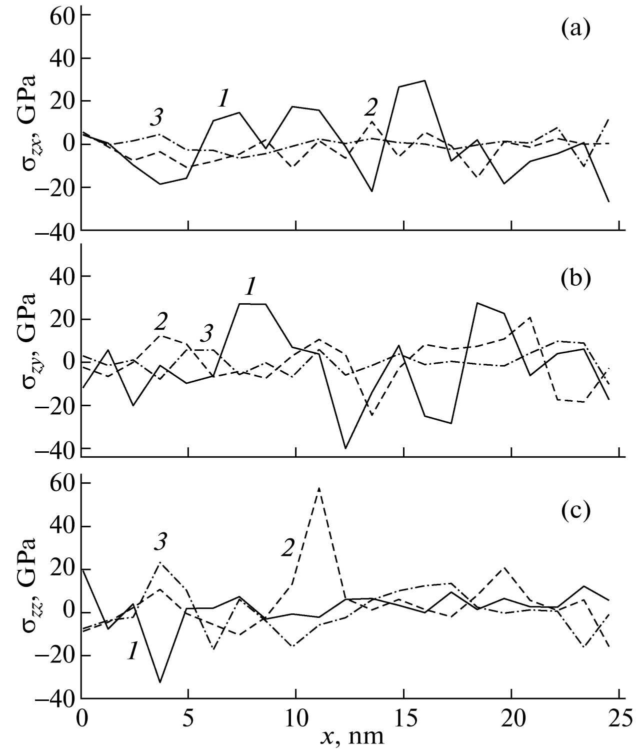

Fig. 6. Distributions of stresses (a) σ_{zx}, (b) σ_{zy}, and (c) σ_{zz} in the graphene sheet over the rows of C atoms passing in the chair direction at 300 (*1*), 1300 (*2*), and 3300 K (*3*).

amount of aluminum by the graphene sheet, Al atoms in each film perform natural vibrations, which are often mismatched for the top and bottom films. At a certain temperature, vibrations of carbon atoms in the graphene sheet, which are chaotic for both films, produce a repulsive effect; as a result, Al atoms leave the surface of the sheet.

Temperature variations of the stresses acting in the plane of the films are illustrated in Fig. 5. The strongest temperature oscillations of stresses are observed for the Al film in system I. With increasing temperature, the stresses in the films decrease and ultimately vanish. The extremely low values of stresses for the Al film in system I are attained at 2300 K, and the film itself can exist even at $T = 3300$ K. The Al films in system II are preserved on graphene up to 1300 K, and at 1800 K, only their remains are observed. For this reason, nonzero stresses are observed in such films up to 1800 K. Stresses σ_{zx} and σ_{zy} produced by horizontal forces in Al films can be considerably (more than an order of magnitude) lower than stresses σ_{zz} produced by vertical forces due to small distances between C and Al atoms.

Let us now see how the presence of a metal film affects the stressed state of graphene. In the case of single-side coating of a graphene sheet by a metal film, stresses σ_{zx} (Fig. 6a) exhibit a much smaller amplitude spread as compared to stresses σ_{zy} (Fig. 6b). Consequently, the interatomic forces acting in the chair direction exceed the forces oriented in the zigzag direction. The middle part of the graphene sheet experiences higher stresses than the edges in the zigzag direction. With increasing temperature, the stress oscillation amplitude decreases, and the amplitude excursion of quantity σ_{zy} remains larger than the analogous characteristic of stress σ_{zx}. At a temperature of 3300 K, for the motion in the *x* direction, the stresses at the middle of the sheet generally become even lower than at the edges. Stress σ_{zz} acting in the plane of the graphene sheet due to vertical forces exhibits slightly different temperature behavior as compared to σ_{zx} and σ_{zy} produced by horizontal forces (Fig. 6c). The maximal absolute values of stress σ_{zz} at $T = 300$ K are observed not in the middle part of the sheet, but at the edges for small values of *x*. At a temperature of 1300 K, a high peak of stress σ_{zz} appears in the middle part of the sheet, while lower peaks of stresses σ_{zz} are located closer to the sheet edges. The high peak is due to vertical displacements of closely packed Al atoms. As a result of such displacements, stress σ_{zx} in the metal film also decreases sharply.

Stresses σ_{zz} in the graphene sheet dissipate upon further heating; however, even at 3300 K, the amplitude of fluctuations in the value of σ_{zz} exceeds the corresponding characteristics of σ_{zx} and σ_{zy} at this temperature.

CONCLUSIONS

The molecular dynamics method is used to test the stability of aluminum films on a graphene sheet heated to 3300 K. The stability of Al films on graphene depends on their number. In the case of single-side coating of the graphene sheet by aluminum, metal atoms are preserved on the graphene surface even at 3300 K, while duplitized coating leads to evaporation of all Al atoms at a temperature of 1800 K. At the first stage (up to $T < 1300$ K), Al atoms are gathered into a dense flat droplet, reducing the film size predominantly in the chair direction. The self-diffusion coefficients of Al atoms in the horizontal and vertical directions considerably increase at $T > 1800$ K in the case of double-sided coating of graphene with aluminum and preserve low values at the top side of the graphene sheet up to 2800 K in the case of single-side coating. The Al atoms are preserved for a longer time on the top side of the graphene sheet, which is reflected in a richer and more intense spectrum of individual vibrations of atoms in the horizontal direction at $T = 1300$ K. The initial predominant contraction of metal films in the chair direction is due to prevailing magnitude of interatomic forces in this direction. For the same reason, the absolute values of stresses σ_{zy} in Al films at $T = 300$ K exceed the corresponding characteristics of stresses σ_{zx}. However, the highest stresses in metal films are primarily due to vertical forces emerging not only due to mutual attraction of Al atoms belonging to different films, but also due to the interaction between graphene and aluminum. The importance of this interaction follows from the high initial stress σ_{zz} for the Al film coating graphene sheet only from one side. With such a coating of the graphene sheet, the stresses from horizontal forces are mainly concentrated in its middle part. The magnitude of the stresses caused by the forces acting in the chair direction is noticeably larger than the corresponding characteristic for the zigzag direction. Heating leads to relaxation of stresses σ_{zx} and σ_{zy}; however, stresses σ_{zz} can be locally enhanced with increasing temperature due to strong convergence of C and Al atoms.

REFERENCES

1. C. Daniel and F. Mucklich, Appl. Surf. Sci. **242**, 140 (2005).
2. K. V. Zakharchenko, A. Fasolino, J. H. Los, and M. I. Katsnelson, J. Phys.: Condens. Matter. **23**, 202202 (2011).
3. A. K. Geim and K. S. Novoselov, Nat. Mater. **6**, 183 (2007).
4. A. A. Balandin, S. Ghosh, W. Bao, I. Calizo, D. Teweldebrhan, F. Miao, and C. N. Lau, Nano Lett. **8**, 902 (2008).
5. J. H. Seol, I. Jo, A. L. Moore, L. Lindsay, Z. H. Aitken, M. T. Pettes, X. Li, Z. Yao, R. Huang, D. Broido, N. Mingo, R. S. Ruoff, and L. Shi, Sciense **328** (5975), 213 (2010).
6. R. Chanchani and P. M. Hall, IEEE Trans. Compon., Hybrids, Manuf. Technol. **11**, 427 (1988).
7. S. H. Lee, M. Park, J. J. Yoh, H. Song, E. Y. Jang, Y. H. Kim, S. Kang, and Y. S. Yoo, Appl. Phys. Lett. **101**, 241909 (2012).
8. L. Wang, J. J. Travis, A. S. Cavanagh, X. Liu, S. P. Koenig, P. Y. Huang, S. M. George, and J. S. Bunch, Nano Lett. **12**, 3706 (2012).
9. Y. Nam, N. Lindvall, J. Sun, Y. W. Park, and A. Yurgens, Carbon **50**, 1987 (2012).
10. Y. Hanaoka, K. Hinode, K. Takeda, and D. Kodama, Mater. Trans. **43**, 1621 (2002).
11. W. C. D. Cheong and L. C. Zhang, Nanotechnology **11**, 173 (2000).
12. O. Kim, Mol. Simul. **31**, 115 (2005).
13. P. M. Morse, Phys. Rev. **34**, 57 (1929).
14. G. C. Abell, Phys. Rev. B **31**, 6184 (1985).
15. J. Tersoff, Phys. Rev. B **37**, 6991 (1988).
16. J. Tersoff, Phys. Rev. Lett. **61**, 2879 (1988).
17. J. Tersoff, Phys. Rev. B **39**, 5566 (1989).
18. S. J. Stuart, A. V. Tutein, and J. A. Harrison, J. Chem. Phys. **112**, 6472 (2000).
19. H. Rafii-Tabar, Phys. Rep. **325**, 239 (2000).
20. T.-H. Fang and J.-H. Wu, Comput. Mater. Sci. **43**, 785 (2008).
21. W. Lee, S. Jang, M. J. Kim, and J.-M. Myoung, Nanotechnology **19**, 285701 (2008).
22. H. J. C. Berendsen, J. P. M. Postma, W. F. van Gunsteren, A. DiNola, and J. R. Haak, J. Chem. Phys. **81**, 3684 (1984).
23. G. E. Norman and V. V. Stegailov, JETP **92**, 879 (2001).
24. A. Y. Kuksin, I. V. Morozov, G. E. Norman, V. V. Stegailov, and I. A. Valuev, Mol. Simul. **31**, 1005 (2005).
25. M. W. Cole, V. H. Cresp, and M. S. Dresselhaus, J. Phys.: Condens. Mater. **22**, 334201 (2010).
26. E. H. Sondheimer, Adv. Phys. **50**, 499 (2001).
27. E. G. Maksimov, D. Yu. Savrasov, and S. Yu. Savrasov, Phys. Usp. **40**, 337 (1997).
28. F. M. Reicha, M. A. El Hiti, and P. B. Barna, J. Mater. Sci. **26**, 2007 (1991).
29. S. Yu. Davydov, Phys. Solid State **54**, 875 (2012).
30. G. K. White and S. J. Collocott, Phys. Chem. Ref. Data **13**, 1251 (1984).

Translated by N. Wadhwa